Simple passive scalar advection-diffusion model

Scott Wunsch*
The James Franck Institute, The University of Chicago, 5640 South Ellis, Chicago, Illinois 60637
(Received 11 March 1998)

This paper presents a simple, one-dimensional model of a randomly advected passive scalar. The model exhibits anomalous inertial range scaling for the structure functions constructed from scalar differences. The model provides a simple computational test for recent ideas regarding closure and scaling for randomly advected passive scalars. Results suggest that high order structure function scaling depends on the largest velocity eddy size, and hence scaling exponents may be geometry dependent and nonuniversal.
[S1063-651X(98)11410-1]

PACS number(s): 47.27.Gs, 05.40.+j

I. INTRODUCTION

There has been much interest in the problem of a randomly advected passive scalar since Kraichnan first proposed a solution for the structure functions that exhibit anomalous scaling [1]. The passive scalar T is governed by the usual equation,

$$\left(\frac{\partial}{\partial t}+\mathbf{u}(\mathbf{x},t)\cdot\boldsymbol{\nabla}\right)T(\mathbf{x},t)=D\nabla^2T(\mathbf{x},t)+F(\mathbf{x},t), \qquad (1)$$

in which D is a diffusion constant and F is an external forcing. If the velocity field is incompressible ($\nabla\cdot\mathbf{u}=0$) and the correlation time is extremely short, the equal time structure functions formed from different powers n of the scalar differences, defined as

$$S_n(\mathbf{r})\equiv\langle[T(\mathbf{x}+\mathbf{r},t)-T(\mathbf{x},t)]^n\rangle \qquad (2)$$

obey equations of the form

$$\mathcal{L}[S_n]=J_n+F_n \qquad (3)$$

in which $\mathcal{L}$ is the Richardson eddy-diffusivity operator, F_n is a forcing term, and J_n is a dissipative term for which an ansatz must be made for closure. In [2], closure was obtained by postulating that the conditional probability of the difference of the Laplacians of the passive scalar at two points is proportional to the difference in the passive scalar values between the points. This leads to even-order structure functions $S_{2n}(r)$, which scale with r, but with scaling indices that are nonlinear functions of n. However, these results have been challenged by others using different techniques to obtain scaling indices in certain limits using perturbative methods [3–6]. A review of the situation is given by Shraiman and Siggia [7].

In this paper I study a model for a passive scalar in one dimension in which the structure functions S_n obey statistical equations with the same form, but with a different eddy diffusivity operator $\mathcal{L}$. The structure functions exhibit scaling because $\mathcal{L}$ is still a scaling operator (by design). The model was previously proposed by myself and others [8], and is based on the linear eddy model of Kerstein [9]. Restricting the model to one dimension makes it possible to numerically study a large range of length scales. The model produces mixing by randomly rearranging the scalar in such a way as to induce scaling in the structure functions. Because the proposed closure of the J_n term in [2] is nothing more than a truncation of the Taylor expansion of the conditional probability, it should be valid (if it is valid) regardless of the form of the operator $\mathcal{L}$.

II. A SIMPLE ONE-DIMENSIONAL MODEL

The principal goal of this paper is to develop a model that is simple enough computationally to permit a large inertial range; hence a one-dimensional scalar field is preferable. However, a one-dimensional incompressible velocity field would be quite dull, so we are forced to choose some other form of mixing that preserves the conservation laws that are the hallmark of incompressibility. Any model in which the advection simply rearranges the scalar field meets these requirements, but such advection is necessarily nonlocal.

The motivation for the particular model I used is developed as follows: Imagine that the one-dimensional scalar field is embedded in a plane. The convection consists of a large eddy in that plane, centered on the scalar field, which rotates one-half turn. This maps the scalar field $T(x)$ onto itself, according to the rule

$$T(x)\rightarrow T(L-x), \qquad (4)$$

where L is the eddy size (centered on $x=\frac{1}{2}L$). Applying one of these eddies in each time step τ, with randomly chosen size and position, along with diffusion, gives a rule for advancing the state of the passive scalar by one time step,

$$T(x,\tau)=T(x,0)+V[T(x,0)]+D\tau\partial_x^2T(x,0) \qquad (5)$$

in which the advection operator $V[T]$ is

$$V[T(x)]\equiv\begin{cases}T(2x_0+L-x)-T(x) & \text{if } x_0\leqslant x\leqslant x_0+L,\\ 0 & \text{otherwise.}\end{cases} \qquad (6)$$

*Electronic address: swunsch@franck.uchicago.edu

The model consists of applying this rule many times, with the size L and position x_0 chosen randomly at each step from appropriate PDFs. All possible x_0 in the system have equal probability, but the eddy sizes L are chosen according to a scaling law with scaling index y

$$P(L)dL = CL^{-y}dL, \tag{7}$$

which generates the scaling behavior within an inertial range determined by the smallest and largest possible values of L: $L_0 < L < L_m$. The ratio of length scales L_m/L_0 plays the role of the Peclet number in this model.

To maintain a state of statistical equilibrium, some forcing is required. In this model, the forcing is done by imposing an overall gradient g on the scalar, as in [4]. A new variable θ is then defined by the deviation from the gradient,

$$\theta(x) \equiv T(x) - gx \tag{8}$$

and structure functions are defined in terms of θ.

III. STRUCTURE FUNCTIONS

A. Structure function equations

I now proceed to determine the analog of the eddy-diffusivity operator $\mathcal{L}$ for this model, along with the forcing function. The scalar difference $\Delta(x,y) \equiv \theta(x) - \theta(y)$ obeys the equation

$$\Delta(x,y;\tau) = D\tau(\partial_x^2 + \partial_y^2)\Delta(x,y;0) + \Psi[\Delta(x,y;0)] \tag{9}$$

when time is advanced by one unit τ. The action of the convective term Ψ on Δ depends on whether x or y (or both) lie within the eddy:

$$\Psi[\Delta(x,y)] \equiv \begin{cases} \Delta(x,y) & x,y \notin [x_0, x_0+L] \\ \Delta(2x_0+L-x,y) + g(L+2x_0-2x) & x \in [x_0, x_0+L], \\ & y \notin [x_0, x_0+L] \\ \Delta(x,2x_0+L-y) - g(L+2x_0-2y) & x \notin [x_0, x_0+L], \\ & y \in [x_0, x_0+L] \\ \Delta(2x_0+L-x,2x_0+L-y) - 2g(x-y) & x,y \in [x_0, x_0+L]. \end{cases} \tag{10}$$

Raising this equation to the nth power and taking the ensemble average gives

$$\begin{aligned} S_n(x-y;\tau) = {} & \langle \Psi^n[\Delta(x,y;0)] \rangle \\ & + nD\tau \langle \Psi^{n-1}[\Delta(x,y;0)](\partial_x^2 + \partial_y^2)\Delta(x,y;0) \rangle \\ & + \cdots \end{aligned} \tag{11}$$

keeping only the lowest order term in $D\tau$. In the diffusive term, we can replace $\Psi[\Delta]$ with Δ, because only a small portion of the scalar field lies within the eddy at that time step (the eddy is another higher order correction). Then the equation becomes

$$S_n(x-y;\tau) = \langle \Psi^n[\Delta(x,y;0)] \rangle + J_n(x,y;0), \tag{12}$$

where

$$J_n(x,y) \equiv nD\tau \langle \Delta(x,y)^{n-1}(\partial_x^2 + \partial_y^2)\Delta(x,y) \rangle \tag{13}$$

as in [1]. The quantity $\langle \Psi^n[\Delta(x,y;0)] \rangle$ can be computed from the definition of Ψ by integrating over the eddy PDFs for x_0 and L. Defining the difference variable $r \equiv x-y$, the result divides into three regions: a dissipative interval ($r \leqslant L_0$), the inertial range ($L_0 \leqslant r \leqslant L_m$), and a large scale region ($r \geqslant L_m$). The structure functions obey the equation

$$\begin{aligned} & \Lambda(S_n(r,\tau) - S_n(r,0)) + \mathcal{L}[S_n(r,0)] \\ & \quad = \Lambda J_n(r,0) + F_n(r,0), \end{aligned} \tag{14}$$

where Λ is the system size. In statistical equilibrium $S_n(r,\tau) = S_n(r,0)$, and this equation is identical in form to Eq. (3). The eddy-diffusivity operator $\mathcal{L}$ and the source $F_n(r)$ differ according to the value of r. For $r \leqslant L_0$, they are

$$\mathcal{L}[S(r)] \equiv -\int_{L_0}^{L_m} P(L)dL \left\{ \int_{L-r}^{L+r} dz S(z) - (r+L)S(r) - (r-L)S(-r) \right\}, \tag{15}$$

$$F_n(r) \equiv \sum_{m=1}^{n} \frac{g^m n!}{m!(n-m)!} \int_{L_0}^{L_m} P(L)dL \left\{ \int_{L-r}^{L+r} dz S_{n-m}(z)(z-r)^m + (L-r)S_{n-m}(-r)(-2r)^m \right\}. \tag{16}$$

In the inertial range, $L_0 \leqslant r \leqslant L_m$, they are

$$\mathcal{L}[S(r)] \equiv -\int_{L_0}^{r} P(L)dL \left\{ \int_{r-L}^{r+L} dz S(z) - 2LS(r) \right\} - \int_{r}^{L_m} P(L)dL \left\{ \int_{L-r}^{L+r} dz S(z) - (r+L)S(r) - (r-L)S(-r) \right\}, \tag{17}$$

$$F_n(r)\equiv\sum_{m=1}^{n}\frac{g^m n!}{m!(n-m)!}\left\{\int_{L_0}^{r}P(L)dL\int_{r-L}^{r+L}dzS_{n-m}(z)(z-r)^m + \int_{r}^{L_m}P(L)dL\left(\int_{L-r}^{L+r}dzS_{n-m}(z)(z-r)^m+(L-r)S_{n-m}(-r)(-2r)^m\right)\right\}. \tag{18}$$

In the large scale region, $r\geqslant L_m$, they are

$$\mathcal{L}[S(r)]\equiv-\int_{L_0}^{L_m}P(L)dL\left\{\int_{r-L}^{r+L}dzS(z)-2LS(r)\right\}, \tag{19}$$

$$F_n(r)\equiv\sum_{m=1}^{n}\frac{g^m n!}{m!(n-m)!}\int_{L_0}^{L_m}P(L)dL\left\{\int_{r-L}^{r+L}dzS_{n-m}(z)(z-r)^m\right\}. \tag{20}$$

B. Solution for $S_2(r)$

The first order structure function S_1 vanishes, so the lowest nontrivial structure function is S_2. It can be determined approximately in both the inertial and dissipative ranges. As a first step, it is necessary to rewrite J_2 by commuting derivatives and using spatial homogeneity:

$$\begin{aligned}J_2&=2D\tau\langle\Delta(\partial_x^2+\partial_y^2)\Delta\rangle\\&=2D\tau\partial_r^2S_2-4D\tau\langle(\partial_x\theta)^2\rangle,\end{aligned} \tag{21}$$

where $D\tau\langle(\partial_x\theta)^2\rangle$ is the mean-square dissipation of the scalar (a constant). This constant can be evaluated by looking at the large scale region (where S_2 must approach a constant) and balancing it with the forcing term $F_2=\frac{2}{3}g^2\langle L^3\rangle$, so that

$$\langle(\partial_x\theta)^2\rangle=\frac{1}{6}\frac{\langle L^3\rangle}{D\tau\Lambda}g^2. \tag{22}$$

This result serves as a check on the accuracy of numerical simulations.

The solution far into the dissipative region ($r\ll L_0$) can then be evaluated by neglecting both $\mathcal{L}$ and F (setting $J_2=0$):

$$S_2(r)\cong\langle(\partial_x\theta)^2\rangle r^2=\frac{1}{6}\frac{\langle L^3\rangle}{D\tau\Lambda}(gr)^2. \tag{23}$$

In the inertial range, the approximate solution is found by balancing the convective term $\mathcal{L}$ against the dissipation term $J_2\cong-4D\tau(\langle\partial_x\theta)^2\rangle$:

$$\mathcal{L}[S_2(r)]\cong-\tfrac{2}{3}\langle L^3\rangle g^2. \tag{24}$$

By assuming a scaling solution, $S_2(r)=A_2r^{\rho_2}$, the convective term becomes

$$\mathcal{L}[A_2r^{\rho_2}]\cong-\frac{A_2L_0^y}{y-1}I(\rho_2,y)r^{2+\rho_2-y} \tag{25}$$

in the limits $L_0/r\to0$ and $r/L_m\to0$. The definite integral $I(\rho,y)$ is defined as

$$\begin{aligned}I(\rho,y)\equiv\frac{1}{1+\rho}\Bigg\{&\int_0^1\frac{dz}{z^y}[(1+z)^{1+\rho}-(1-z)^{1+\rho}\\&-2(1+\rho)z]+\int_0^1\frac{dz}{z^{3+\rho-y}}[(1+z)^{1+\rho}\\&-(1-z)^{1+\rho}-2(1+\rho)z^{1+\rho}]\Bigg\}\end{aligned} \tag{26}$$

and can be evaluated numerically. The first integral in I diverges at the lower limit for $y>3$, setting an upper limit on the scaling range. (For $y>3$ the lower limit must be replaced by L_0/r, and the ultraviolet region determines the solution.) Since this term balances a constant, the scaling is fixed at $\rho_2=y-2$ (which only makes sense for $y>2$) and the solution is

$$S_2(r)=\frac{2}{3}\frac{(gL_m)^2}{(2-\rho_2)I(\rho_2,y)}\left(\frac{r}{L_m}\right)^{\rho_2}, \tag{27}$$

where I have evaluated $\langle L^3\rangle$ explicitly.

These solutions for S_2 compare very well with the numerical results in both the inertial and dissipative ranges (see Fig. 1).

C. Inertial range scaling for even-order structure functions

In the inertial range, the scaling of higher even-order structure functions is determined in the same way as S_2:

$$\mathcal{L}[S_{2n}(r)]\cong J_{2n}(r). \tag{28}$$

The closure assumption for J_{2n} made in [1] is that

$$J_{2n}(r)=nC_nJ_2\frac{S_{2n}}{S_2} \tag{29}$$

with $C_n=1$. The generalized form with $C_n\neq1$ was suggested in [10]. Assuming scaling functions for S_{2n} with indices ρ_{2n}, leads to the result that the scaling indices satisfy

$$I(\rho_{2n},y)=nC_nI(\rho_2,y). \tag{30}$$

This result can be used (in principle) to evaluate C_n given numerically measured ρ_{2n}. Unfortunately, the sensitivity of

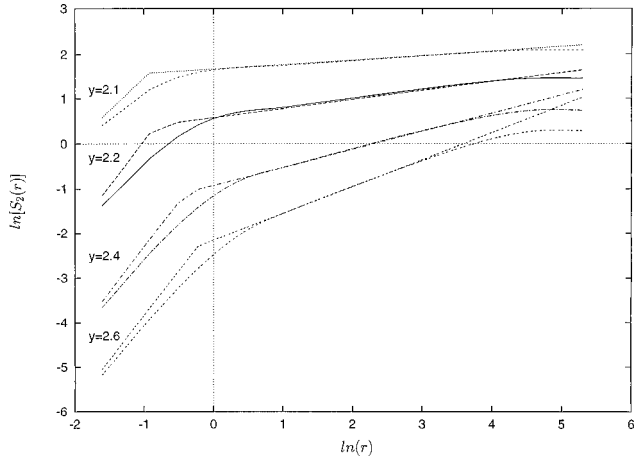

FIG. 1. Second order structure functions $S_2(r)$ on a log-log plot, for $L_m=200$ and four values of the scaling parameter y. Smooth curves are numerical simulation data; straight lines represent the analytic scaling solution in two regimes (inertial and dissipative ranges).

I to ρ prevents this from being very accurate. However, the numerical results for the exponents and C_n (measured independently) are consistent with this result, indicating that the scaling is indeed set by balancing the convective term $\mathcal{L}$ against the dissipation term J_{2n}.

D. Odd-order structure functions

Odd-order structure functions exhibit scaling only in the dissipative range. Because the eddy-diffusivity operator $\mathcal{L}$ differs depending on whether it operates on an odd or even function of r, the inertial range scaling solution exists only for even-order structure functions. Odd-order functions are positive scaling functions at small r, but pass through zero in the inertial range and then approach zero from below at large r. This behavior of the odd structure functions is peculiar to this particular model and differs from physical passive scalars.

E. Dissipation range scaling

At small enough length scales the dissipative terms dominate the scaling. In this (dissipative) range the J_n term dominates the solution. It is convenient to rewrite it as

$$J_n(r)=2D\tau\partial_r^2 S_n(r)-n(n-1)D\tau \times\langle\Delta^{n-2}[(\partial_x\theta)^2+(\partial_y\theta)^2]\rangle. \tag{31}$$

Balancing the two parts of J_n against each other will lead to a solution if the conditional probability

$$G(\Delta,x-y)\equiv\langle[(\partial_x\theta)^2+(\partial_y\theta)^2]|\Delta\rangle \tag{32}$$

can be determined. In a purely dissipative system, G can be determined from a Taylor expansion of Δ at small separations: $\Delta\cong r(\partial_x\theta)$, which implies $G=2\Delta^2/r^2$. However, the presence of convection competes with the smoothing effects of diffusion and generates higher terms in the Taylor expansion of Δ. Given this fact, a reasonable closure approximation (which is supported numerically) is

$$G(\Delta,r)=a+\frac{b\Delta}{r}+\frac{c\Delta^2}{r^2}, \tag{33}$$

where a, b, and c are constants. The assumed r dependence is necessary to generate a solution with regular scaling.

Assuming a regular scaling solution, $S_n(r)=A_n r^n$, and expressing the unknown constants in terms of A_2 (calculated above) and A_3 (unknown), the constants A_n are found to obey

$$A_n=A_{n-2}A_2+\frac{A_3}{A_2}A_{n-1}. \tag{34}$$

Hence all higher order structure functions are expressible in terms of S_2 and S_3. Unfortunately, no analytic solution for S_3 has been found. However, in the absence of any spatial asymmetry (which is generated by the gradient forcing used in this model) the odd-order structure functions would vanish and the solution would be

$$S_{2n}(r)=S_2^n(r), \tag{35}$$

which has regular scaling but non-Gaussian statistics.

IV. NUMERICAL RESULTS

A computational model was created by discretizing the dynamical equation for $T(x)$. The advective term is handled straightforwardly, since it is just a rearrangement of the values of $T(x)$. Diffusion was done subsequent to the advection process in each time step, using a second-order implicit finite differences scheme. An overall gradient was applied to generate forcing, and periodic boundary conditions for the fluctuating field $\theta(x)$ were used. The system was evolved to a state of statistical equilibrium before any averaging computations were done. Equilibrium was indicated by the establishment of stable (analytically known) values of $\langle(\partial_x\theta)^2\rangle$ and $S_2(r)$. Structure functions were computed by taking space-time averages over the entire simulation.

Simulations were conducted in a system with 50 000 grid points and a grid spacing of $dx=0.1$. The smallest eddy size was $L_0=2$, permitting a significant dissipative interval. The largest eddy size was either $L_m=200$ or $L_m=500$, allowing for inertial range scaling over two orders of magnitude. The imposed gradient was $g=0.01$. The eddy scaling exponent was varied between $y=2.1$ and $y=2.8$ for $L_m=200$, and between $y=2.1$ and $y=2.4$ for $L_m=500$. The number of time steps varied between 3×10^7 and 10^8. A large number of time steps is needed to suitably average over the eddy size probability distribution $P(L)$, especially for larger L_m and y. In addition, several simulations were conducted with large diffusion constants $D\tau=0.02$ to study the dissipative range solution.

Second order structure functions S_2 have been computed analytically and can be compared directly with simulation results. Figure 1 shows S_2 as a function of r on a log-log plot (base e) for $L_m=200$ and four values of y. The smooth curves show the simulation data (50 data points each). The analytic results are shown as two straight lines (one for the dissipative region, and one for the inertial range). There are no free parameters. The agreement is good (within 5% in the heart of the inertial range) except at the inertial range boundaries, where the analytic calculation has no validity.

Figure 2 shows higher even-order structure functions on a log-log plot for $y=2.4$ and $L_m=500$. Scaling holds over a

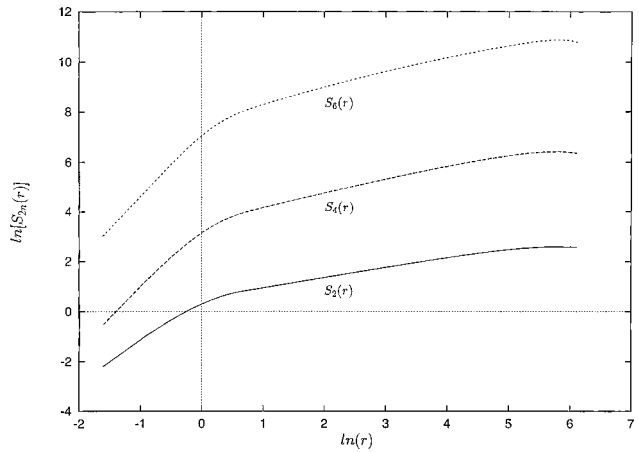

FIG. 2. Higher order structure functions $S_{2n}(r)$ on a log-log plot, revealing scaling behavior in the inertial range. Data from the simulation with $y=2.4$ and $L_m=500$.

range from approximately $r=2$ to $r=200$. Figure 3 shows the even-order scaling indices ρ_{2n} as a function of n for five values of y. The error bars represent the range of observed values over several simulations with different initial conditions. The scaling indices appear to be independent of the upper length scale L_m. The second order indices ρ_2 lie within 3% of the theoretical values $y-2$. The deviation from regular scaling ($\rho_{2n}=n\rho_2$) is quite pronounced. For larger y, the scaling exponents appear to approach a constant value (dependent on y) as n increases.

A. Probability distribution functions

Figure 4 shows the probability distribution function for Δ on a log-linear scale for several values of r from the $y=2.4$, $L_m=200$ simulation. The core of the PDF, defined roughly by $|\Delta|\leqslant gL_m$ ($gL_m=2$), is peaked. The slight asymmetry between positive and negative Δ is due to the imposed gradient.

In the inertial range the PDF exhibits exponential tails for $\Delta\gg gL_m$:

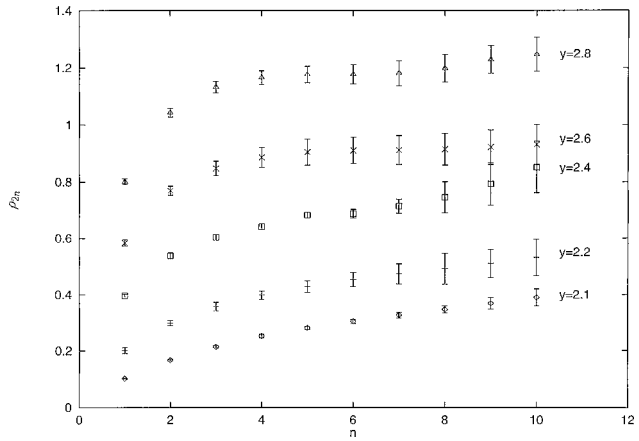

FIG. 3. Inertial range structure function scaling exponents ρ_{2n} as a function of n for five values of y. These simulation data agree with the analytically known result $\rho_2=y-2$ for $n=1$. The data suggest that the exponents may approach a constant value as $n\to\infty$.

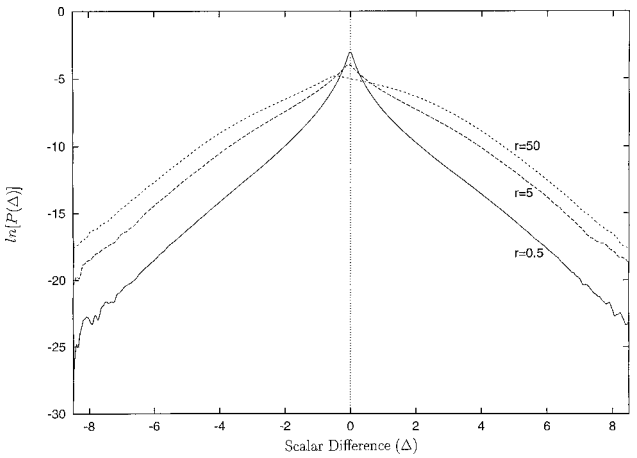

FIG. 4. Probability distribution function $P(\Delta)$ of scalar differences Δ for three separations r, from the $y=2.4$, $gL_m=2$ simulation. The tails ($|\Delta|>gL_m$) of the distribution appear to be exponential, with a slope that is independent of r.

$$P(\Delta,r)\cong A(r)e^{-c|\Delta|} \tag{36}$$

where c is independent of the separation r. The exponential tails have also been derived in another model in a particular limit [13]. This form of the PDF suggests that, for large n, the structure function scaling exponents ρ_{2n} approach a constant independent of n. The structure functions obey

$$\frac{S_{2n}}{S_{2n-2}}=\frac{2n(2n-1)}{c^2} \tag{37}$$

in the limit of large n. The PDF's and the structure functions can both be used to independently estimate c, and the results are shown in Fig. 5 (as a function of ρ_2). The two sets of data represent the two different values of L_m, $L_m=200$ and $L_m=500$.

The exponential tails can be understood in terms of a random walk of fluid elements. To generate a particular scalar difference Δ, fluid elements initially separated by a dis-

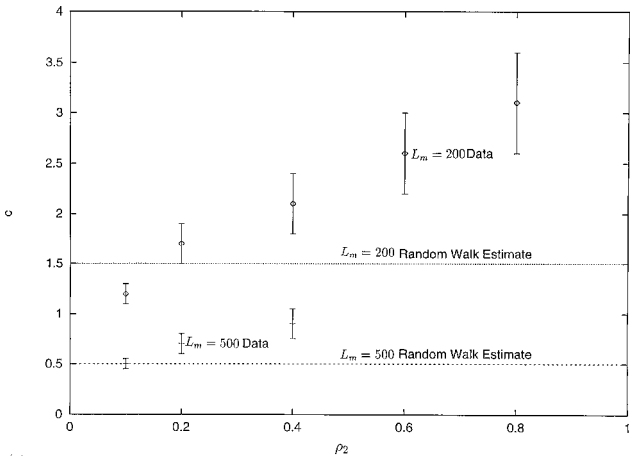

FIG. 5. Slopes c of the tails of the PDF $P(\Delta)$ measured from simulation data for $L_m=200$ and $L_m=500$. The straight lines represent the Lagrangian random-walk estimate of c. The dependence on ρ_2 arises because large eddies become less frequent as ρ_2 increases.

tance of order Δ/g must be brought close together. Since the largest correlated motion in the system is of size L_m, scalar differences larger in magnitude than gL_m can only be generated by the uncorrelated action of several eddies. This behavior is essentially a random walk, and the multiplication of probabilities leads to the exponential PDF.

To be more quantitative, consider the probability for the motion of a fluid element along a Lagrangian trajectory from position zero to position x. For simplicity assume that all eddies are the same size L. To move a distance x with $(m-1)L \leqslant x \leqslant mL$ (for integer m) will typically require the point to be moved by m eddies, each carrying it a distance of order L. However, the probability that the point will lie within a particular eddy is L/Λ, and these probabilities multiply

$$P(x \sim mL) \sim \left(\frac{L}{\Lambda}\right)^m. \tag{38}$$

The motion must occur quickly, in (order of magnitude) m steps, or else diffusion will cause the fluid element to equilibrate with its new environment. By assuming the two points involved in constructing Δ move independently, this probability can be converted to a PDF for Δ by using $x \sim \Delta/g$ regardless of the separation r. The result is

$$P(\Delta) \sim e^{-c\Delta}, \tag{39}$$

$$c \equiv \frac{1}{gL} \ln\left(\frac{\Lambda}{L}\right). \tag{40}$$

Assuming that each eddy is of size L_m suggests estimates of $c=1.5$ for $L_m=200$ and $c=0.5$ for $L_m=500$. These values are shown as straight lines in Fig. 5, and are in qualitative agreement with the data. Of course, not all eddies are of size L_m; in fact the number of large eddies decreases as ρ_2 increases. This results in the trend of increasing c shown in Fig. 5.

Once two fluid elements have come close together, they become subject to correlated motions. This is presumably the source of the r dependence in the prefactor $A(r)$ of the exponential tail. Correlated motions have a weak influence on the PDF tail, and cannot alter its exponential character. Also, there is a slight asymmetry between Δ and $-\Delta$ in the prefactor; this is attributed to the fact that producing a negative Δ requires the two points to pass by each other (in one dimension), and during this time their motion is correlated.

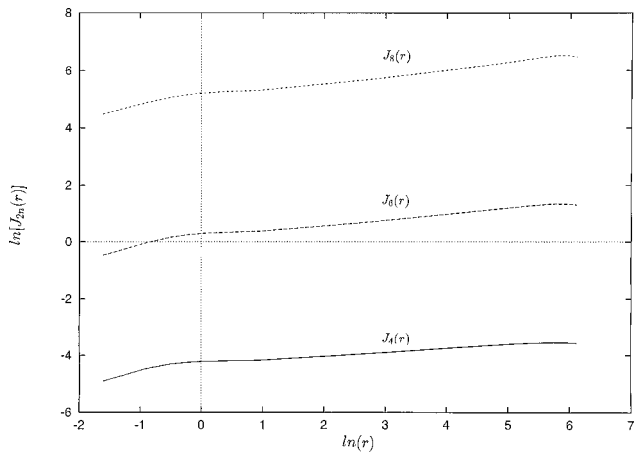

FIG. 6. Dissipation function J_{2n} on a log-log plot, indicating scaling behavior in the inertial range. Data from the simulation with $y=2.4$ and $L_m=500$.

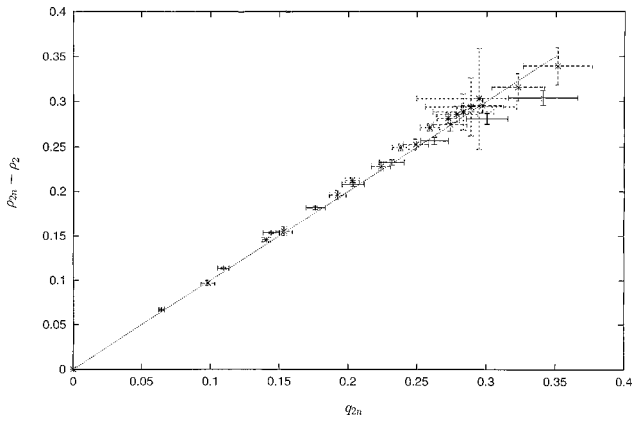

FIG. 7. Inertial range scaling exponents q_{2n} for the dissipation functions J_{2n} compared to the structure function scaling exponents ρ_{2n}. Kraichnan's closure ansatz requires $q_{2n}=\rho_{2n}-\rho_2$, and the simulation data are consistent with this result.

B. Kraichnan's closure ansatz

To test the closure ansatz in [1] and evaluate the constants C_n, the dissipation functions J_{2n} were computed directly from the simulation data. Rather than use the Laplacian, J_{2n} was rewritten by commuting derivatives as

$$J_{2n}(r) = 2D\tau\partial_r^2 S_{2n}(r) - 2n(2n-1)D\tau \times \langle \Delta^{2n-2}[(\partial_x\theta)^2 + (\partial_y\theta)^2]\rangle. \tag{41}$$

In the limit $D\tau \to 0$, only the second term on the right side remains. In actual simulations, the first term makes a finite contribution that makes it more difficult to determine the inertial range scaling. So in practice only the second term (approximated using finite differences) was used as a surrogate for J_{2n} in the inertial range. Figure 6 shows numerical simulation values for J_{2n} for the $y=2.4$, $L_m=500$ simulation. In the inertial range, the J_{2n} scale with r and have scaling indices q_{2n} which, by the closure ansatz, ought to satisfy

$$q_{2n} = \rho_{2n} - \rho_2. \tag{42}$$

Figure 7 shows that this part of the closure ansatz holds, by plotting q_{2n} versus $\rho_{2n}-\rho_2$ for the $L_m=500$ simulations.

The constants C_n can be computed using $C_n = J_{2n}S_2/nJ_2S_{2n}$ and averaging over the inertial range (C_n is approximately constant over the region averaged). The resulting values do not appear to depend on any parameters of the system other than y (a weak dependence on L_m is suspected but not detectable). Figure 8 shows computed values for C_n averaged over several simulations. The deviation from $C_n=1$ is small but significant, contradicting the ansatz of [1]. The growing values of C_n at small ρ_2 suggest near-regular scaling in this limit, at least for moderate values of n. This is consistent with the scaling exponents in Fig. 3. The

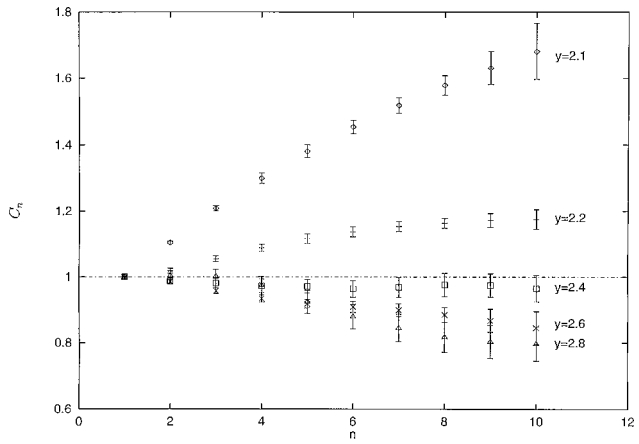

FIG. 8. Closure constants of proportionality C_n, defined by $J_{2n}(r)=nC_nJ_2S_{2n}/S_2$, from simulation data for several y. Kraichnan's closure ansatz requires $C_n=1$, which is inconsistent with the data. For larger y, C_n decreases with n, suggesting scaling exponents might approach a constant value at large n. For smaller y, C_n increases with n, suggesting near-regular scaling for moderate values of n. Both trends are consistent with the scaling exponents shown in Fig. 3.

intermediate case $\rho_2=0.4$ lies very close to the Kraichnan prediction of $C_n=1$. For larger ρ_2, C_n decreases with n, consistent with the scaling exponents approaching a constant value (as in Fig. 3).

In [2], the closure ansatz in [1] is derived from an assumption about a conditional probability, namely, that

$$H(\Delta,x-y)\equiv\langle(\partial_x^2+\partial_y^2)\Delta(x,y)|\Delta(x,y)\rangle = \left(\frac{J_2}{2D\tau S_2}\right)\Delta. \tag{43}$$

This conditional probability $H(\Delta,r)$ has be computed numerically in the simulations. Figure 9 shows $H(\Delta)$ as a function of Δ, normalized by $J_2/2D\tau S_2$, for $\rho_2=0.1$ and both $L_m=200$ and $L_m=500$. Two values of r are shown for each simulation. The resulting averages lie very close to $H(\Delta)=\Delta$ for small Δ, as assumed in [2]. However, they deviate from the straight line at $|\Delta|\cong 2gL_m$. This is approximately the point at which correlated motion becomes unimportant and the dynamics are controlled by the ''random walk'' described in the previous section. The failure of Kraichnan's ansatz appears to be due to the existence of a finite upper size of the inertial range, L_m, which is much smaller than the system size. Other values of ρ_2 exhibit a similar behavior.

C. Dissipative range closure ansatz

The conditional probability $G(\Delta)$ needed for closure in the dissipative range is shown in Fig. 10 for several values of r (from the simulation with $D\tau=0.02$). The conditional probabilities are well approximated by the parabola

$$G(\Delta,r)=a+\frac{b\Delta}{r}+\frac{c\Delta^2}{r^2} \tag{44}$$

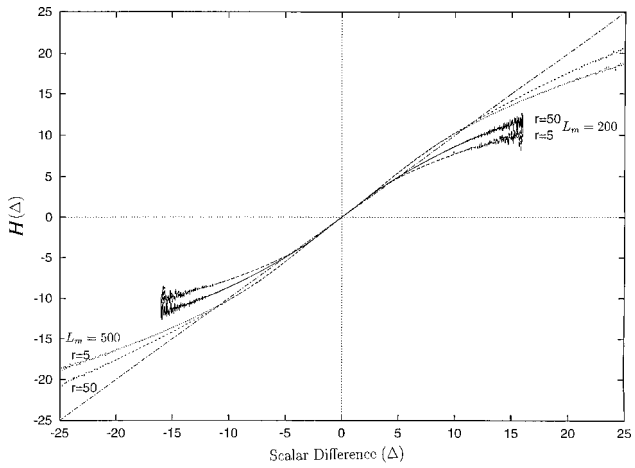

FIG. 9. Conditional probability $H(\Delta,x-y)\equiv\langle(\partial_x^2+\partial_y^2)\Delta(x,y)|\Delta(x,y)\rangle$ as a function of the scalar difference Δ for two values of L_m and two separations $r=x-y$. Data are taken from the $y=2.1$ simulations. H is normalized so that $H=\Delta$ is the Kraichnan ansatz. The ansatz is in good agreement with the data for small values of Δ, but the data deviate for $|\Delta|>2gL_m$ ($g=0.01$). This is approximately the largest value of Δ that can be generated by a single large eddy; larger values are exponentially unlikely (see Fig. 4).

with $a\cong 4\times10^{-7}$, $b\cong 2\times10^{-3}$, and $c\cong 1.99$. These values are consistent with the independently known values of A_2 and A_3.

The structure functions are given by $S_n(r)=A_nr^n$, and the constants A_n are shown in Fig. 11. In addition, the calculated values $A_n=A_{n-2}A_2+(A_3/A_2)A_{n-1}$ are also shown, using the analytically known value of A_2 and the value of A_3 determined from fitting $S_3(r)$. The deviations from the analytic solution at large n are possibly due to the neglected terms F_n and $\mathcal{L}$ in the equation for the structure functions.

V. CONCLUSIONS

Simulations done using this simple model appear to contradict the assumptions made in [1] and [2]. Specifically, the

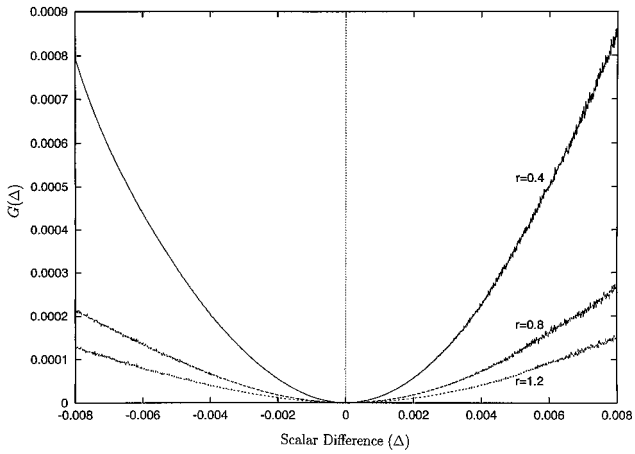

FIG. 10. Conditional probability $G(\Delta,x-y)\equiv\langle[(\partial_x\theta)^2+(\partial_y\theta)^2]|\Delta(x,y)\rangle$ as a function of the scalar difference Δ for several values of r in the dissipative subrange. Data from the diffusion-dominated simulation. The parabolic form is consistent with the small-scale closure ansatz proposed in this paper.

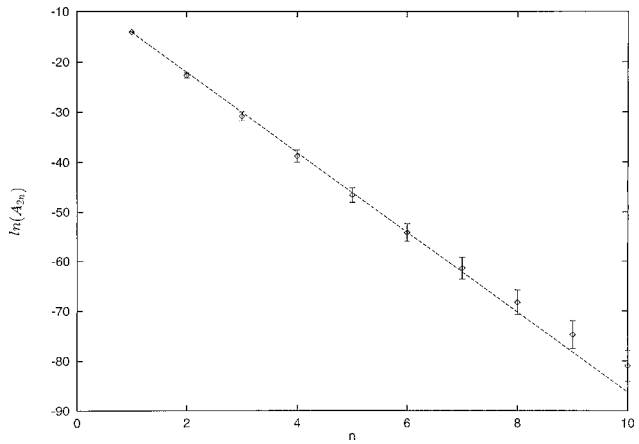

FIG. 11. Structure function coefficients A_{2n} as a function of n for the dissipative range regular-scaling solution, $S_{2n}=A_{2n}r^{2n}$. The data points were determined by fitting the simulation data. The straight line is the analytic solution, with the unknown parameter A_3/A_2 determined by fitting the numerical data for $S_3(r)$.

conditional probability studied in [2] is not a linear function of Δ, deviating at large values ($|\Delta| \geqslant 2gL_m$). The deviation arises because the largest velocity eddy in the system (L_m) is much smaller than the system size. This finite length scale effect should cause scaling exponents ρ_{2n} to deviate from the values predicted in [1] for sufficiently large n. The constants of proportionality C_n proposed in [10] deviate from 1, growing with n for small ρ_2 but shrinking with n at large ρ_2 (in contradiction to the predictions of [11] and also the simulations of [12]). The finite upper length scale induces exponential tails in the probability distribution function of scalar differences Δ, leading to scaling exponents that approach a constant for sufficiently large n. The order n at which this occurs should be controlled by the geometric parameter gL_m and the model parameter ρ_2. Hence the scaling exponents would not be universal. Exponential tails and constant scaling exponents at large n have also been shown analytically in 1D compressible flow in the limit $\rho_2 \to 0$ [13].

The separation of length scales (between the largest eddy size and the system size) required for exponential tails in the scalar difference PDF can be achieved in pipe flow. The finite diameter of the pipe limits velocity eddies to this size, while the pipe itself can be much longer (analogous to this 1D model). Recent experiments on pipe flows [14] have revealed PDF's of scalar values with exponential tails. No attempt has been made to study scalar differences, but the arguments of the previous section suggest that exponential tails in the scalar value PDF would imply exponential tails in the scalar difference PDF. If true, this would force structure function scaling exponents in turbulent pipe flow to approach a constant (nonuniversal) value at large n.

For a flow in a cube (or similar geometry), the largest velocity eddy would be comparable to the system size, and large-scale mixing could occur under the correlated motion of a single large eddy. Hence the mechanism for generating exponential tails in the PDF would not exist, and there is no reason to expect that scaling exponents ρ_{2n} would approach a constant at large n. The structure function scaling exponents of the passive scalar might therefore be geometry dependent.

ACKNOWLEDGMENTS

It is a pleasure to acknowledge useful discussions with L. P. Kadanoff, G. Falkovich, D. Lohse, P. Constantin, M. Chertkov, T. Zhou, and N. Schoegerhofer. This work was supported in part by the Fannie and John Hertz Foundation. We also utilized MRSEC shared facilities under NSF-DMR Grant No. 9400379.

[1] R. Kraichnan, Phys. Rev. Lett. **72**, 1016 (1994).
[2] R. Kraichnan, V. Yakhot, and S. Chen, Phys. Rev. Lett. **75**, 240 (1995).
[3] K. Gawedzki and A. Kupianen, Phys. Rev. Lett. **75**, 3834 (1995).
[4] Boris I. Shraiman and Eric D. Siggia, C. R. Acad. Sci., Ser. IIb: Mec., Phys., Chim., Astron. **321**, 279 (1995).
[5] M. Chertkov, G. Falkovich, I. Kolokolov, and V. Lebedev, Phys. Rev. E **52**, 4924 (1995).
[6] M. Chertkov, G. Falkovich, and V. Lebedev, Phys. Rev. Lett. **76**, 3707 (1996).
[7] Boris I. Shraiman and Eric D. Siggia (unpublished).
[8] L. P. Kadanoff, S. Wunsch, and T. Zhou, Physica A **244**, 190 (1997).
[9] A. R. Kerstein, J. Fluid Mech. **231**, 261 (1991).
[10] E. Ching, V. S. L'vov, and I. Procaccia, Phys. Rev. E **54**, 4520 (1996).
[11] E. Ching, Phys. Rev. Lett. **79**, 3644 (1997).
[12] A. Fairhall, B. Galanti, V. L'vov, and I. Procaccia, Phys. Rev. Lett. **79**, 4166 (1997).
[13] M. Chertkov, I. Kolokolov, and M. Vergassola Phys. Rev. Lett. **80**, 512 (1998).
[14] J. E. Guilkey, A. R. Kerstein, P. A. McMurtry, and J. C. Klewicki, Phys. Rev. E **56**, 1753 (1997).